*Desalination and Water Treatment*
www.deswater.com

doi:10.5004/dwt.2018.22265

113 (2018) 121–130
May

# Scale-inhibition and adsorption capacity due to a synergistic effect between a magnetic field and graphene oxide–carbon nanotube composite

Lili Jiang[a,*], Liefei Pei[a], Haitao Yu[b], Zongshu Zou[c], Fengman Shen[c], Xingang Hou[a]

[a]*School of Material Science and Technology, Lanzhou University of Technology, Langongping Road, Lanzhou730050, Gansu Province, China, Tel. & Fax +86 24 83681545, email: jianglili2002@163.com (L. Jiang), Tel. +86 931 2976378, Fax +86 931 2976702, email: 992632787@qq.com (L. Pei), Tel. +86 931 2976378, Fax +86 931 2976702, email: houxg1958@163.com (X. Hou)*
[b]*Department of Medical Laboratory, The First Hospital of Lanzhou University, No. 1, Donggang Road, Chengguan District,Lanzhou 730000, Gansu Province, China, Tel. +86 0931 8626421, Fax +86 0931 8619797, email: yuhaitao7707@163.com (H. Yu)*
[c]*School of Metallurgy, Northeastern university, No.3-11, Wenhua Road, Heping District, Shenyang, Liaoning Province, China, Tel. & Fax +86 24 83681545, email: zouzs@mail.neu.edu.cn (Z. Zou), shenfm@ mail.neu.edu.cn (F. Shen)*

Received 25 October 2017; Accepted 27 March 2018

**ABSTRACT**

A synergistic effect between a magnetic field and sulfhydryl- and amino-modified graphene oxide/oxidized multi-walled carbon nanotubes ($NH_2$-SH-GO/o-MWCNTs) that leads to scale inhibition in circulating water as well as the adsorption of lead ions and phenol is investigated. The composite was used to adsorb $Pb^{2+}$ and phenol from circulating water and the results were analyzed to investigate the effect of varying the magnetic field intensity on various parameters including equilibrium adsorption capacity, pH, conductivity, activation energy, and relative change in intramolecular energy and free water proportion. The results show that the equilibrium adsorption capacity with respect to $Pb^{2+}$ gradually increases with increasing magnetic field intensity. At a magnetic field intensity of 0.54 T, the equilibrium adsorption capacity reached 130 and 27.36 mg/g for $Pb^{2+}$ and phenol, respectively. The synergistic effect caused the molecular activation energy in the circulating water to increase, while the intramolecular energy decreased. Due to the copious production of hydrogen bonds, collisions with scale-forming ions declined so that magnetic field was also able to play a role in scale inhibition. The synergistic effect between magnetic field and $NH_2$-SH-GO/o-MWCNT is thus able to inhibit scale formation and adsorb pollutants from circulating water.

*Keywords:* Carbon nanotubes; Water treatment; GO; Magnetic field

## 1. Introduction

The treatment of industrial wastewater has been an important problem since the start of industrial development. Industrial wastewater is discharged by various industries including those associated with mining, metallurgical processing, machinery manufacture, chemical engineering (e.g. pesticide, paint, dye production, etc.), the electronics industry, and instrument manufacturing [1]. According to a survey by Nriagu [2], millions of tons of heavy metals are directly discharged into the natural environment every year including arsenic ($1.25\times10^5$ tons), cadmium ($3.9\times10^4$ tons), copper ($1.47\times10^5$ tons), mercury ($1.2\times10^4$ tons), lead ($3.46\times10^5$ tons), and nickel ($3.81\times10^5$ tons). The quantity discharged has also shown a growing trend in successive years. Wastewater bearing heavy metals and phenol often contains substances that are non-biodegradable and have long-term toxic effects. Thus, they can enter the human body, accumulate, and cause various illnesses [3,4]. Some metal ions circulating in industrial water systems can also corrode the walls of their confining tubes due to electrochemical effects which shortens the serviceable lives of the tubes. Scale produced in tubes is another problem as it decreases the cross-sectional area of the tube and reduces the flow of the water. This can lead to blockage of the flow of the coolant which decreases the cooling efficiency and

*Corresponding author.

even lead to overheating [5–7]. Hence, it is of fundamental importance to investigate and develop highly efficient methods of treating wastewater.

The traditional methods of treating wastewater containing heavy metals and phenol mainly involve chemical precipitation [8], electrochemical methods [9], treat by alum [10], and membrane separation techniques [11]. However, these methods are highly constrained in their practical application, including the length of the technological process, high cost, and poor circular utilization. Adsorption methods are the most common and effective among the current methods for water purification as they are generally simple to operate and have high efficiency [12].

Graphene oxide (GO) is a two-dimensional layered carbon nanomaterial with a thickness corresponding to a single atom [13]. Carbon nanotubes (CNTs) have tubular structures that are seamless and curled about a central shaft according to a certain helical angle [14]. As they are both nanomaterial, GO and CNTs exhibit large specific surface areas. Their special structures mean that they have plenty of activated adsorption sites and they are also chemically very stable. Thus, they possess the basic properties of potential adsorption materials [15]. Chen prepared an effective adsorbent that diamine functionalized mesoporous silica on multi-walled carbon nanotubes to remove heavy metals in aqueous solution [16]. Adsorption kinetics could be well described by pseudo-second-order kinetic equation and the prepared adsorbent has good adsorption capacity. Yu synthesized a novel 3D composite of graphene oxide-starch by the hydrothermal treatment. And this porous 3D graphene oxide-starch composite exhibited high adsorption capacities of 108.68, 32.12, 46.28, 41.76 and 38.168 mg/g for Pb(II), Cu(II), Cd(II), Yb(III) and Nd(III) from aqueous solutions, respectively [17]. Jie recently prepared a magnetic GO/chitosan ternary composite material using a 'one-pot' solvothermal method [18]. The composite material was found to contain a large number of oxygen-containing functional groups and $Fe_3O_4$ magnetic particles loaded onto layers of GO which have a favorable magnetic separation effect. The maximum adsorption capacity of the composite material with respect to sulfadiazine was found to be 79.23 mg/g. Zhu used a simple solution method to conduct sulfhydryl modification of natural montmorillonite soil by using a modifier consisting of (3-mercaptopropyl)trimethoxysilane(MPTS)[19]. The result of adsorption experiments subsequently showed that the maximum adsorption capacity of the trimethoxysilane with respect to Cd(II) was 39 times than that of the montmorillonite. Kumar Ray prepared a new adsorbent by integrating chitosan with crosslinked polymethacrylic acid (PMA) and nano sized halloysite nanotube (HNT). And the adsorbent capacity was 357.4 and 341.6 mg/g for single Pb(II) and Cd(II), respectively [20]. McKay synthesized an effective adsorbent by carbon nanotubes (CNT) modified with four generations of poly-amidoamine dendrimer (PAMAM, G4) to remove $Cu^{2+}$ and $Pb^{2+}$ from aqueous solution [21]. Yu applied diiodocarbene to modify oxidized multi-walled carbon nanotube (ox-MWCNT-CI2) by reaction of ox-MWCNT with iodoform under a strong alkaline condition. And the adsorbent showed higher efficiency for Pb(II) [22]. Yu prepared triethanolamine functionalized multi-walled carbon nanotube (MWCNT-TEA) and utilized for the removal of Pb(II) from aqueous solutions [23].

The main methods used to inhibit scale formation in industrial engineering include chemical (adding chemical agents), physical (including irradiation and microwave-treatment), and physicochemical methods. In the latter, the circulating water is treated using ultraviolet light and ozone. There are many disadvantages to the aforementioned methods including secondary pollution of the environment, high energy consumption, and high construction costs [24]. Magnetic treatment, however, is a very promising method of scale prevention which integrates various functions including scale prevention and removal, sterilization, and corrosion inhibition. Its primary advantages are: low investment costs, operational simplicity, and low toxicity/pollutant production [25]. The effect of the magnetic treatment technique is mainly manifested in terms of: (i) a change in ionic hydration diameter, and (ii) an increase in the viscosity coefficient of the solvent. As a result, ionic activity decline which reduces the amount of calcium salts precipitated [26]. After being subjected to magnetic treatment, two solutions used to precipitate $CaCO_3$ in solution was found to more rapidly generate the aragonite form of the precipitate (which has a loose, metastable structure that is unstable) and which could be subsequently drained to improve pollution discharge [27]. The solubility of calcium salts in water increases after magnetic treatment, which means that some of the scale can be re-dissolved. To the best of our knowledge, a technique combining the use of a magnetic field and adsorbent has not been reported to date.

The present study aims to treat circulating water using a synergistic effect between a magnetic field and GO/CNT composite material. We also investigate whether the synergistic effect plays a role in scale inhibition and promotes the adsorption of metal ions and organic substances onto the absorbent. First, the adsorbent composite material-consisting of sulfhydryl-and amino-modified GO/oxidized multi-walled carbon nanotubes ($NH_2$-SH-GO/o-MWCNTs) was prepared and characterized using transmission electron microscopy (TEM), Fourier transform infrared (FT-IR) spectroscopy, and X-ray photoelectron spectroscopy (XPS). The synergistic effect between the prepared composite materials as adsorbents and the magnetic field was imposed on the circulating water containing $Pb^{2+}$, $Ca^{2+}$ and phenol. On this basis, the effect of using magnetic fields of different intensity was investigated. Various parameters were determined including the equilibrium adsorption capacity of the adsorbent, the pH, conductivity, molecular activation energy, and the relative changes in the intramolecular energy and proportion of free water.

## 2. Experimental methods

### *2.1. Materials and reagents*

The multi-walled CNTs were purchased from Shenzhen Nanotech. Port Co. Ltd., (China). According to the manufacturer, the diameters of MWCNTs are in the range 10–20 nm and their specific surface areas are in the range 100–160 $m^2/g$. Ultra-pure water was used for solution preparation. Lead nitrate and phenol were purchased from Tianjin Fu Rui Technology Co. Ltd. (China). Nitric acid, sulfuric acid,

hydrazine, and acetone (purity > 99.5%) were purchased from Big Alum Chemical Reagent Factory (China). The (3-mercaptopropyl)trimethoxysilane was purchased from Beijing Biological Technology (China). All of the chemicals were of analytical grade and used without further purification.

### 2.2. Characterization techniques

TEM (type JEM-2010, operating at 200 kV) was used to characterize the morphology of the samples. FT-IR spectra were recorded using a Nexus-870. All of the samples were prepared by mixing KBr with the MWCNTs or modified MWCNTs and spectra recorded over the 400–4000 $cm^{-1}$ range. XPS was used to determine the chemical composition of the surface of the samples using AlK radiation. The resulting XPS spectra were deconvoluted using XPS peak analysis software. The concentration of lead ions was determined using an Hitachi Z-5000 atomic absorption spectrophotometer (AAS), and that of phenol was found using an ultraviolet–visible spectrophotometer (model VU-1000). Specific surface area of all samples was measured by specific surface area instrument (Type 3H-2000PS2). All of the water used though the experiment was produced using an ultra-pure water system (Ulupure, UPD-I-20T).

### 2.3. Experimental equipment and water quality analysis

The equipment used to investigate the synergistic effect between the magnetic field and $NH_2$-SH-GO/o-MWCNTs are shown in Fig. 1. The system is composed of a water tank, water pump, valve, water-heating tank, adjustable permanent magnet, and a water meter. The pump was used to circulate the water which was heated by passing it through the water-heating tank (adjustable using a temperature controller). The adjustable magnet equipment was manufactured by Shenzhen Yitian Magnetic & Devices Co., Ltd, China, and was operated over a range of 0–0.8 T.

Artificial hard water was prepared by dissolving $CaCl_2$, $Pb(NO_3)_2$, and phenol in the circulating water. Conductivity, pH, molecular activation energy, relative change in intramolecular energy, and proportion of free water were selected as measurement objectives. A pH meter (type Delta320, Mettler-Toledo Ltd.) was used to measure the pH value of the circulating water and a conductivity meter to measure its conductivity (type Delta326, Mettler-Toledo Ltd.). Viscosity was determined using a viscometer (produced by Shanghai Fangrui Devices Co., Ltd.). Nuclear magnetic resonance experiments were carried out using a Bruker Avance AVIII 400 spectrometer equipped with a standard 5 mm probe at 400 MHz. The sample temperature was set to 298 K and kept constant to within ±0.1 K.

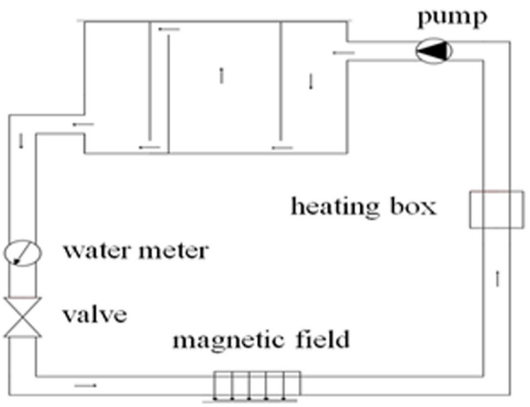


Fig. 1. The devices used to investigate the synergistic effect between a magnetic field and $NH_2$-SH-GO/o-MWCNTs.

### 2.4. Preparation of the $NH_2$-SH-GO/o-MWCNTs

#### 2.4.1. Preparation of GO/o-MWCNTs

A weighed sample of MWCNTs (1 g) was added to a three-necked bottle together with 30 ml of concentrated sulfuric acid and 10 ml of concentrated nitric acid to remove impurities. Then, the mixture was stirred ultrasonically for 3 h at 60°C. The suspension produced was filtered, rinsed with deionized water until the pH value reached 7, and then dried in a vacuum oven at 80°C for 12 h. The product obtained was oxidized MWCNTs (o-MWCNTs).

Graphene oxide was prepared according to a modified Hummers' method. First, natural graphite (2 g) was dispersed in a three-necked bottle with 46 ml of sulfuric acid keeping the temperature below 5°C. The mixture was stirred until dissolution was complete, and then sodium nitrate (1 g) and potassium permanganate (6 g) slowly added. The mixture was then stirred for 2.5 h. The mixture was then placed in a water bath kettle at 85°C and stirred for 24 min. Then, hydrogen peroxide (40 ml, wt 30%) was added and left for 5 min. The mixture was separated and the solid washed with deionized water until the pH value of the product reached neutrality. Finally, the product was treated with ultrasonication, centrifuged, and dried in a vacuum oven for 24 h at 80°C. The product obtained was GO.

Weighed portions of GO (0.1 g) and o-MWCNTs (0.2 g) were dispersed in 100 ml of absolute alcohol and treated for 2 h with ultrasound. The mixture was placed into a three-necked bottle and treated with ultrasound for another 2 h. Finally, it was filtered, washed with absolute alcohol several times, and then dried in a vacuum oven for 12 h at 80°C. The product obtained is the GO/o-MWCNTs component used in the next stage.

#### 2.4.2. Preparation of $NH_2$-SH-GO/o-MWCNTs

A portion of GO/o-MWCNTs (200 mg) was added to 40 ml of absolute alcohol at 25°C. Then, 4 ml of acetic acid and 8 ml of MPTS was added and the solution left for 24 h, after that, 100 ml of acetone was slowly dispersed into the solution. The SH-GO/o-MWCNTs produced were filtered and washed several times with ultra-pure water. A sample of the SH-GO/o-MWCNTs (100 mg) was dispersed in 50 ml of absolute alcohol. The mixture was stirred vigorously and 10 ml of hydrazine hydrate added. Then, the mixture was further stirred for 6 h. Subsequently, the composite was filtered and washed. Finally, the product was dried in a vacuum oven at 80°C for 8 h. The product finally obtained was the $NH_2$-SH-GO/o-MWCNTs.

*2.5. Investigating the synergy between $NH_2$-SH-GO/o-MWCNTs and a magnetic field*

Ten liters of ultra pure water were placed in the circulating system and the system adjusted to furnish the required conditions (a flow rate of 0.17 m/s, initial adsorbate concentration of 50 mg/l, and temperature of 30°C). Our initial experiments showed that the magnetic field had its optimal effect on scale inhibition under the conditions. The permanent magnet was adjusted to yield different magnetic field intensities. The magnetic variation experiments were conducted on a circulating water system where a known concentration (50 mg/l) of $NH_2$-SH-GO/o-MWCNTs was flowing. Water samples was withdrawn after 5, 15, 25, 35, 45, 60, 75, 100, 140, 195, 285, 405, 525, and 685 min and used to determine pH, viscosity, and surface tension. On this basis, much information could be calculated, including the relative change in intramolecular energy, the variation in the molecular activation energy, and the relative change in the proportion of free water. Additionally, small amounts of water were taken at 0 and 685 min to measure the peak widths of nuclear magnetic resonance of circulating water using the NMR spectrometer. Afterwards, the relative change in the proportion of free water in the circulating system was further calculated using Eq. (1) [28]:

$$\frac{\Delta C}{C_0} = \frac{C - C_0}{C_0} = \frac{\Delta v_{1/2}^0 - \Delta v_{1/2}}{\Delta v_{1/2}} \tag{1}$$

where $C$ is the proportion of free water after magnetic treatment, $C_0$ the initial proportion of free water, and $\Delta C/C_0$ the relative change in the proportion of free water. In addition, $\Delta v_{1/2}$ is the experimental peak width (at half height) and $\Delta v_{1/2}^0$ the initial peak width (at half height). Similarly, the change in the intramolecular energy can be found in Eq. (2) [29]:

$$\frac{E^{\text{inner}} - E_0^{\text{inner}}}{E_0^{\text{inner}}} = \frac{S - S_0}{S_0} = \frac{T - T_0}{T_0} \tag{2}$$

where $E^{\text{inner}}$ refers to the intramolecular energy (J), $S$ to entropy (J/mol/K), and $T$ to surface tension (N/m). As before, a subscript '0' refers to an initial value (before application of the magnetic field) and unsubscripted values to those after magnetic treatment. Thus, $(E^{\text{inner}} - E_0^{\text{inner}})/E_0^{\text{inner}}$ is the relative change in the intramolecular energy caused by the magnetic field. A certain amount of circulating water was taken to measure the concentration of $Pb^{2+}$ ions and phenol. The amount of lead and phenol adsorbed by the adsorbent was subsequently calculated according to Eq. (3) [30]:

$$q_e = \frac{(C_0 - C_e)V}{M} \tag{3}$$

where $q_e$ is the quantity adsorbed at equilibrium by the adsorbent (mg/g), $C_0$ and $C_e$ are the initial and equilibrium concentration of adsorbate (mg/l), respectively, $V$ is the volume of the solution (l), and $M$ is the mass of adsorbent (g).

If $E$ and $E_0$ denote the activation energies of the experimental water and ultra-pure water (kJ/mol), respectively, then the relative change in activation energy $\Delta E/E_0$ can be calculated from the viscosity of the solution by Eq. (4) [31]:

$$\frac{\Delta E}{E_0} = \frac{E - E_0}{E_0} = \frac{\ln\eta - \ln\eta_0}{\ln\eta_0 - \ln\left(hN_A/V_m\right)} \tag{4}$$

where $\eta$ and $\eta_0$ are the viscosities of the solution and ultrapure water, respectively (m·Pa·s), $h$ is Planck's constant ($h = 6.626\times10^{-34}$), $N_A$ is Avogadro's constant ($N_A = 6.02\times10^{23}$ $mol^{-1}$), and $V_m$ is the molar volume of the liquid (l/mol).

## 3. Results and discussion

### *3.1. TEM*

Fig. 2 displays TEM images of the original MWCNTs, purified MWCNTs, GO, and $NH_2$-SH-GO/o-MWCNTs. It can be clearly seen from Fig. 2a that the original MWCNTs have tubular structures with diameters of about 20 nm and whose surfaces are smooth with a few catalyst impurities upon them. The impurities show serious signs of agglomeration, implying that as original MWCNTs were not well dispersed, they needed to be purified. The length of original MWCNTs is greater than 5 μm and the specific surface area is 80–140 $m^2/g$ measured by specific surface area instrument. Fig. 2b illustrates that the shortened multi-walled CNTs had been purified by the use of the mixed acids (hardly any catalyst impurity is apparent). And the length of purified MWCNTs is shored and about greater than 1 μm and the specific surface area is 100–160 $m^2/g$. As a result of the oxidation treatment, the surfaces of the multi-walled CNTs had become rough, showing lots of grooves and pits. In addition, the tail ends have become unpacked, implying that the agglomeration of MWCNTs had been reduced because of the oxidation treatment. The reason was that surfaces of MWCNTs carried numerous oxygen-containing functional groups (including carboxyl and hydroxyl) which improved the dispersity of MWCNTs. Fig. 2c shows that the natural graphite has a laminar structure and its widths is of about 400–500 nm. The specific surface area is about 100–130 $m^2/g$. As shown in Fig. 2d, GO has a massive thin sheet structure with numerous folds and the layers are closely combined with widths of about 10–20 μm. The specific surface area is about 120–170 $m^2/g$. The gaps among the graphite layers have clearly increased under the oxidizing effect of the oxidizing agents. Fig. 2e shows that the GO becomes connected with the purified MWCNTs to form a spatial stereochemical structure where MWCNTs are inserted into the layers of GO. And the specific surface area is about 140–180 $m^2/g$. A large number of MWCNTs have adsorbed onto the surface of GO, which directly indicates that the synthesis of $NH_2$-SH-GO/o-MWCNTs has been successful.

### *3.2. FT-IR analysis*

Fig. 3 presents FT-IR spectra of GO/o-MWCNTs and $NH_2$-SH-GO/o-MWCNTs. It can be seen from Fig. 3a that an obvious absorption peak due to a stretching vibration appears at 1622 $cm^{-1}$ which can be assigned to C=C stretching in the CNTs and GO [32]. This result showed that the basic structures of CNTs and GO were not damaged despite being subjected to oxidation by the strong acids. The spectrum of the $NH_2$-SH-GO/o-MWCNTs revealed that there were three new peaks at 1245, 750, and 720 $cm^{-1}$, which cor-

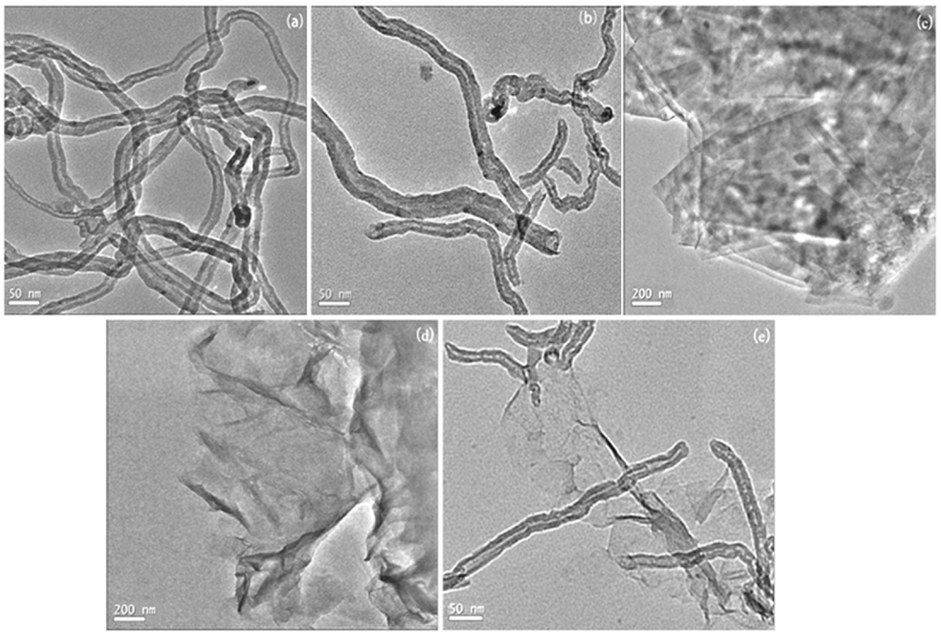


Fig. 2. TEM images, (a) original MWCNTs, (b) o-MWCNTs, (c) graphite, (d) graphene oxide, and (e) $NH_2$-SH-GO/o-MWCNTs.

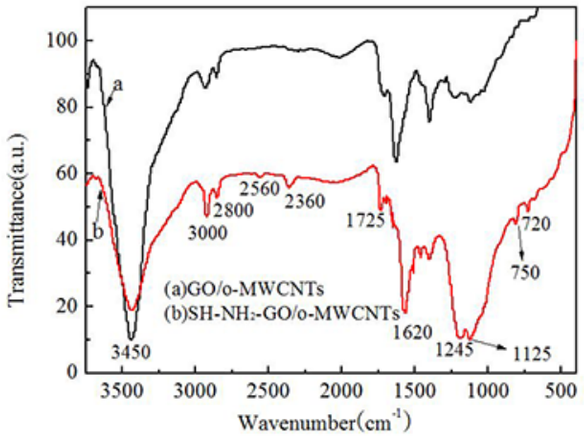


Fig. 3. FT-IR spectra of GO/o-MWCNTs (a) and $NH_2$-SH-GO/o-MWCNTs (b).

respond to the stretching vibration of Si–O, Si–C, and Si–N bonds, respectively. The silicon element derives from the MPTS. The occurrence of Si-O bond implied that the MPTS had connected to the oxygen-containing groups on the surfaces of the CNTs or GO, while the appearance of Si–N peak showed that amino groups also connected with the MPTS. The above results directly verify that amino and sulfhydryl groups were loaded onto the surfaces of the CNTs or GO. Fig. 3b shows the peaks occurring at 3450 $cm^{-1}$ and 1725 $cm^{-1}$ correspond to the stretching vibrations of O–H and C=O, respectively. This was because a large number of hydroxyl and carboxyl groups were introduced during the oxidation of the graphite and purification of the CNTs. Additionally, there is a weak peak at 2560 $cm^{-1}$, which belongs to a stretching vibration of S–H, implying that sulfhydryl groups occur in $NH_2$-SH-GO/o-MWCNTs [33]. The aforementioned results indicate that amino and sulfhydryl groups are loaded on the surfaces of the CNTs and GO to successfully synthesize the composite material $NH_2$-SH-GO/o-MWCNTs.

Table 1
Energies, peak areas, and elemental percentages found for the $NH_2$-SH-GO/o-MWCNTs

| Element | Energy (eV) | Peak area (%) | Percentage (%) |
|---|---|---|---|
| C1s | 284.39 | 74.07 | 82.55 |
| O1s | 530.66 | 16.29 | 11.76 |
| N1s | 400.25 | 4.44 | 2.76 |
| S2p | 164.51 | 2.96 | 1.56 |
| Si2p | 101.32 | 2.22 | 1.37 |

### 3.3. XPS analysis

XPS is a method typically used to analyze the surface functional groups of composite materials. Table 1 displays the elements found in the $NH_2$-SH-GO/o-MWCNTs and their percentages. As can be seen, C, O, N, S, and Si occur with percentage of 82.55%, 11.76%, 2.76%, 1.56%, and 1.37%, respectively. The oxygen content is high which implies that there are numerous oxygen-containing groups on the surfaces of the $NH_2$-SH-GO/o-MWCNTs. The occurrence of S and Si also reveals that sulfhydryl groups can be found in the $NH_2$-SH-GO/o-MWCNTs. Fig. 4a shows there are five elements in $NH_2$-SH-GO/o-MWCNTs. The strong peak at 284.8 eV corresponds to the element C in the CNTs, while

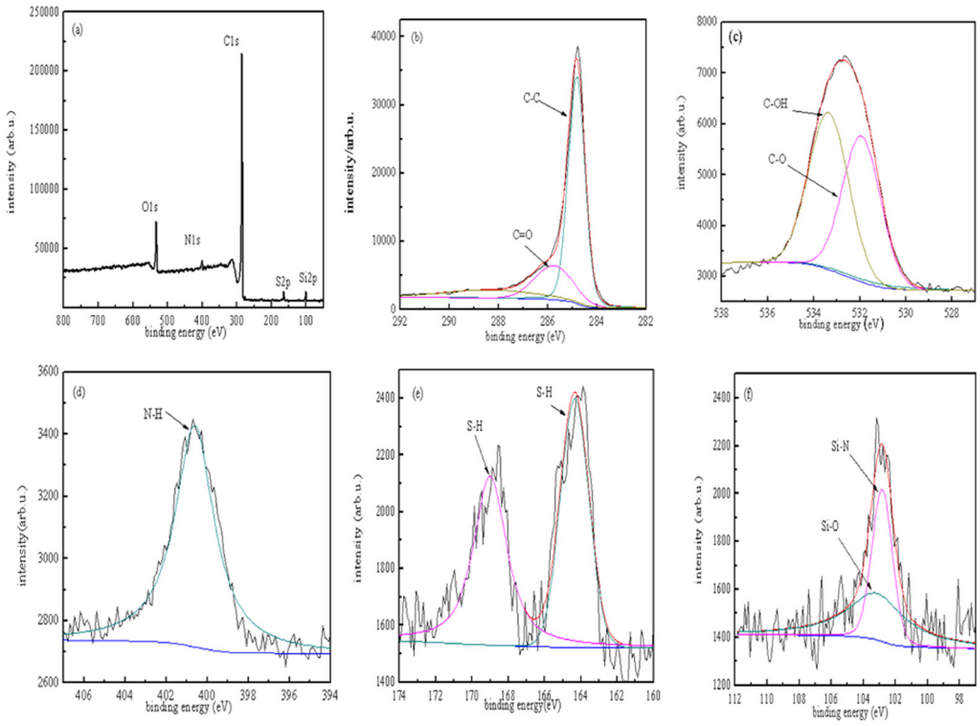


Fig. 4. A wide XPS scan of the $NH_2$–SH–GO/o-MWCNTs composite is shown in (a) and more detailed views are also shown of the (b) C1s, (c) O1s, (d) N1s, (e) S2p, and (f) Si2p peaks. The experimental data was fitted to Gaussian forms (assigned to specific chemical bonds, as indicated) and the best fits plotted in the figures.

the peaks at 530.66 and 400.25 eV correspond to O1s and N1s, respectively. In contrast, the weak peaks at 164.51 and 101.32 eV belong to S2p and Si2p, respectively.

Fig. 4b reveals that the C1s energy spectrum in $NH_2$-SH-GO/o-MWCNTs can be divided into two Gaussian peaks at 284.39 and 286.6 eV, which correspond to C=C in the MWCNTs or GO and C=O in carboxyl group, respectively. As shown in the sub-peak spectrum of O1s (Fig. 4c), the Gaussian peaks at 531.94 and 533.35 eV correspond to C–O and C–OH, respectively, which is consistent with the results of an analysis of the C1s data in the energy spectrum. The occurrence of these oxygen-containing groups directly verifies that the surfaces of the CNTs or GO had been oxidized. These oxygen-containing groups provide more adsorption sites for the adsorption of pollutants. Fig. 4d shows the Gaussian peak measured for N1S, which implies that there are N–H groups in the $NH_2$-SH-GO/o-MWCNTs, while Fig. 4e indicates that there are also sulfhydryl groups in the composite material. Fig. 4f reveals that the Gaussian peaks corresponding to Si–O and Si–N were detected at 103.48 and 102.78 eV, respectively, indicating that the MPTS was successfully incorporated onto the surfaces of the CNTs and GO and the sulfhydryl groups were connected with the amino groups. These results confirm the FT-IR results.

### *3.4. Relative variation of free water proportion*

Fig. 5 illustrates relative variation in of free water proportion varies at different magnetic field intensities. It can be seen from the figure that the original concentration of target ions was 50 mg/l after 685 min of magnetic treatment while the relative change in the proportion of free water in the circulating system without magnetic treatment was 41.01%. When the magnetic field intensity was 0.27 T, the original concentration of target ions was 50 mg/L and the relative change in the free water proportion declined to 22.88%. The fall in the relative change in proportion of free water indicates that the proportion of free water molecules in the circulating water dropped because of the magnetic treatment while the proportion of associated water rose. Therefore, more ions were transformed into hydrated ions. This reduces the probability of calcium carbonate scale, and so the results indirectly verify that the magnetic field has a scale-inhibiting effect on the circulating water. The relative change in the proportion of free water decreased constantly with increasing magnetic field intensity, which implies that a more significant scale-inhibition effect results from stronger magnetic fields [34]. When the original concentration of target ions was increased to 70 mg/l, although the proportion of free water still declined, the degree was significantly lower than the original concentration of 30 and 50 mg/l. This illustrates that larger concentrations did not give rise to a better magnetic treatment effect. This is because the increase in the number of the hydrogen bonds is smaller due to increasing the original concentration of the target ions so that more free water molecules occurred in the circulating water. Thus, more target ions exist in the form of ions in the circulating water, which increases the probability that calcium and carbonate ions will combine and therefore reduces the scale-inhibiting effect of the magnetic field.

When the initial concentration rose to 90 mg/l, the phenomenon was more evident. Therefore, the relative changes in the proportion of free water decreases under the synergistic effect between the magnetic field and $NH_2$–SH–GO/o-MWCNTs. This indicates that the proportion of free water molecules declines and more target ions exist as hydrated ions. This facilitates the production of hydrogen bonds and reduces the rate of mutual collision between scale-producing ions so that the magnetic field exerts a scale-inhibiting effect [35].

### 3.5. Change in adsorption quantity with magnetic field intensity

Fig. 6 shows how the quantity of target pollutants adsorbed changes with magnetic field intensity. Fig. 6a illustrates the results for lead ions. Without magnetic treatment, the adsorption capacity for lead ions increased rapidly at first and then stabilized. The adsorption amount reached 76.37 mg/g at 35 min and the adsorption process gradually stabilized. When the magnetic field intensity was 0.27 T, adsorption capacity for lead ions also rapidly rose at first and then stabilized. In this case, adsorption amount corresponds to 99.90 mg/g, which is far larger than that of without a magnetic field. This result clearly shows that magnetic field can promote the adsorption process of $NH_2$–SH–GO/o-MWCNTs for lead ions. It is apparent that magnetic field favors the adsorption process for lead ions due to a synergistic effect between magnetic field and $NH_2$–SH–GO/o-MWCNTs. The phenomenon becomes more significant as magnetic field intensity increases. In particular, the adsorption amount for lead ions reached 130 mg/l at 0.54 T, which is about twice than that of without magnetic field. The above results prove that magnetic field promotes the adsorption process for lead ions due to a synergistic effect between the magnetic field and $NH_2$–SH–GO/o-MWCNTs. The effect was optimal when the magnetic field intensity was 0.54 T.

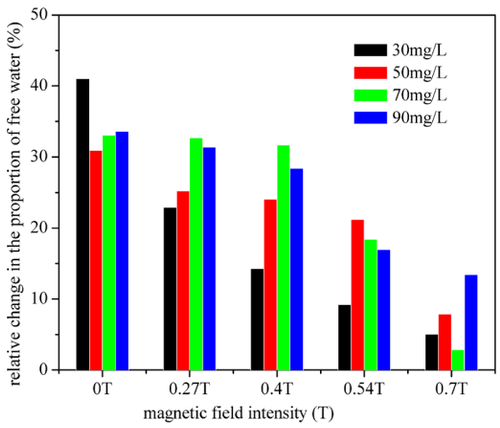


Fig. 5. The effect of magnetic field intensity on the relative change in the proportion of free water.

Fig. 6b shows similar results for phenol by $NH_2$–SH–GO/o-MWCNTs. Compared with Fig. 6a, magnetic field in this case can inhibit the adsorption for phenol onto the adsorbent. As time passed, the quantity of phenol adsorbed onto the adsorbent without a magnetic field rose at first and then stabilized. The amount of phenol adsorbed reached 39.71 mg/l after 35 min, which is far lower than that for lead. This indicates that phenol competes with lead ions and the adsorption capacity of $NH_2$-SH-GO/o-MWCNTs for lead ions is higher than that for phenol. With increasing magnetic field intensity, the quantities of phenol adsorbed by $NH_2$–SH–GO/o-MWCNTs increase at first and then stabilized. However, the quantity adsorbed is far lower than that without a magnetic field, implying that magnetic field inhibits the adsorption process for phenol. This phenomenon becomes increasingly more significant as the magnetic field intensity increases. This is because $Pb^{2+}$ mainly occurs as hydrated ions in water and the polarity of the moving water molecules weaken under the effect of the external magnetic field which reduces their electrostatic attraction to the positive ions [36]. Additionally, the charged ions exhibit as crew type circular motion as they are affected by a Lorentz force. Therefore, it is relatively easy for $Pb^{2+}$ions to rid themselves of the constraints placed on them by the

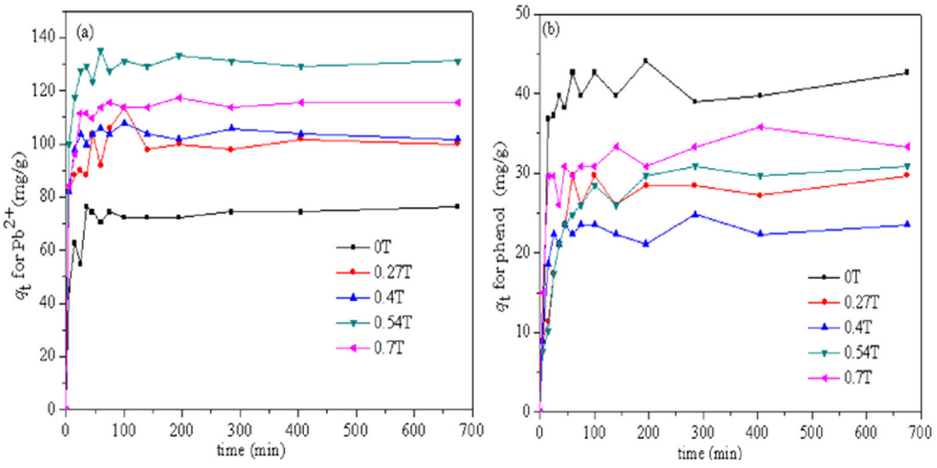


Fig. 6. The effect of magnetic field intensity on adsorption capacity towards (a) $Pb^{2+}$ and, (b) phenol.

moisture. As a result, they become small hydrated ions or single ions, which increase the probability of colliding with the electronegative parts of the adsorbent. Thus, $Pb^{2+}$ is more readily adsorbed. When the magnetic field intensity is 0.7 T, the adsorption quantities decrease slightly. Large water-containing molecular clusters hinder the adsorption effect and thereby reduce the quantity adsorbed by the adsorbent. Thus, the quantity of phenol adsorbed was far lower than that of $Pb^{2+}$ [37]. Although it contains some polar groups, the adsorbent is mainly composed of nonpolar covalent bonds, such as C–C and C=C. Thus, the adsorbent shows the characteristics of nonpolar molecules. That is, it is easy to adsorb nonpolar molecules. However, the adsorption of phenol by the adsorbent is mainly realized through complexing reactions with the polar bonds on the surface because phenol is a polar molecule [38]. The quantity of phenol adsorbed is low because there are only a few polar bonds on the surface. Phenol and water both consist of polar molecules and the former ionizes weakly. Phenol combines with water molecules to form close water–molecule clusters via a mutual orientation force which aggravates the inclusion phenomenon. Therefore, phenol combines with the adsorbent with some difficulty.

### 3.6. The changesin pH and conductivity

To investigate the synergistic effect on the solution's pH and conductivity, we measured the pH value and conductivity for different magnetic field intensities: 0, 0.27, 0.4, 0.54, and 0.7 T (a flow rate of 0.17 m/s and original concentration of 50 mg/l was used throughout). Fig. 7 displays the results. It can be observed from the figure that the pH of the circulating water dramatically fluctuated in the range 5.34–4.89 when the circulating water was not subjected to a magnetic field (0 T). This suggests that the quality of the circulating water was unstable. This may be related to the fact that $CO_2$ (in the air) was constantly dissolving into the circulating water and thus changing the pH value [39]. When the magnetic field intensity was 0.27 T, the pH of the circulating water tended to be more stable, maintaining a value in the region of 5.1. It became increasingly more obvious that the pH value became more stable as the magnetic field intensity became larger. The above result shows that a magnetic field can stabilize the pH of the circulating water. Scale is less likely to occur in circulating water that has a more stable pH value, which indirectly verifies that the magnetic field has a scale-inhibiting effect on the circulating water.

Fig. 7(b) reveals the effect of magnetic field intensity on conductivity. As the figure shows, the conductivity of the circulating water fluctuated only slightly when the magnetic treatment was not applied. Thus, the number of conductive ions in the circulating water hardly changed during the experiment. When a magnetic field of 0.27 T was applied to the circulating water, the conductivity rapidly increased to 285 μS/cm after 15 min. As the duration of the magnetic treatment was further prolonged, the conductivity fluctuated only slightly. The increase in conductivity shows that the number of conductive ions had increased. Thus, ions that would have become the nuclei of calcium carbonate crystals were transformed into free ions or hydrated ions thus inhibiting the scale-formation effect [40]. The phenomenon became increasingly more noticeable with further increases in magnetic field intensity. This proves that the magnetic field had a scale-inhibiting effect on the circulating water. The above results verify that the magnetic field is still able to inhibit scale formation in the presence of the synergistic effect between magnetic field and $NH_2$-SH-GO/o-MWCNTs.

### 3.7. Molecular activation energy and intramolecular energy

Fig. 8 shows the effect of magnetic field on molecular activation energy and intramolecular energy. The changes in molar energy ($\Delta E$) and activation energy ($\Delta E$) of the liquid satisfy Eq. (5) [39]:

$$\Delta E = -\Delta E' = -(E' - E_0')$$
$$\Delta E = RT\ln(\eta/\eta_0) \quad (5)$$

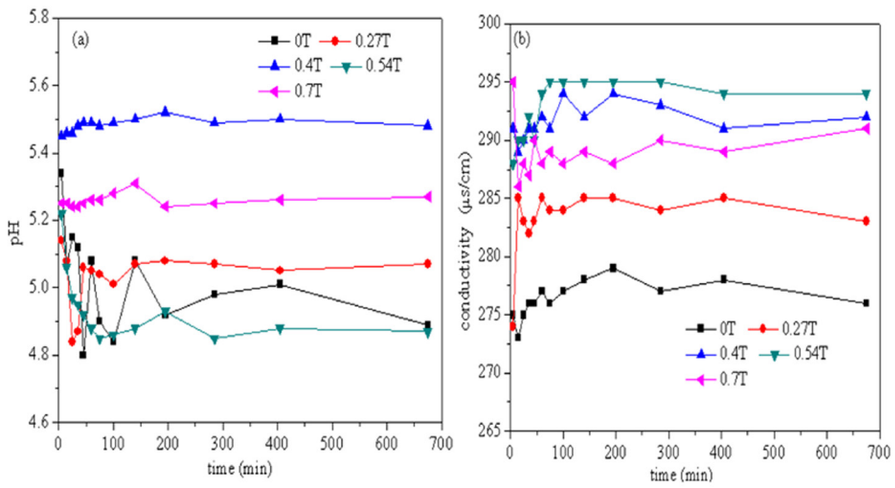


Fig. 7. The effect of magnetic field on (a) pH value, and (b) conductivity.

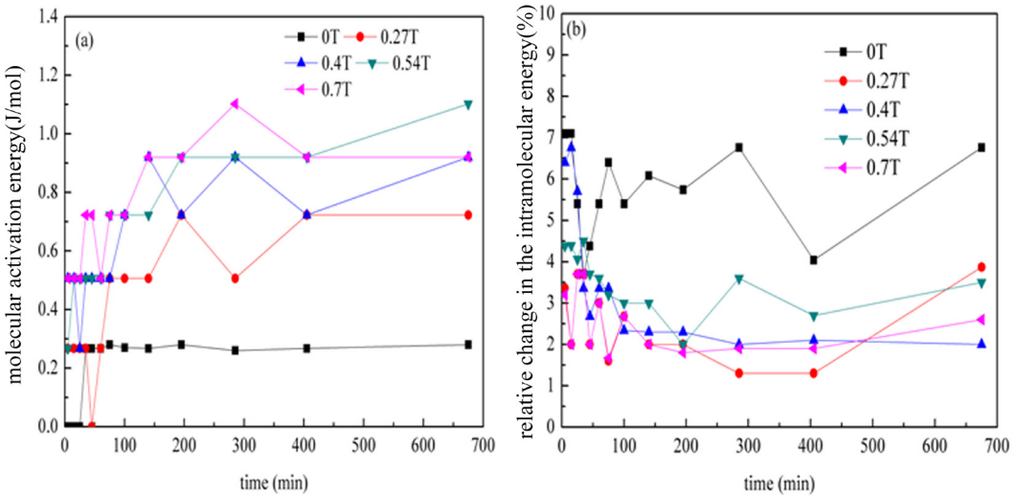


Fig. 8. The effect of magnetic field on (a) molecular activation energy, and (b) intramolecular energy.

where η and $\eta_0$ represent viscosities of the circulating water with and without the magnetic field (mPa·s), respectively; $E'$ and $E'_0$ mean molar activation energy of circulating water with and without the magnetic field (J/mol); and $\Delta E$ represents the change in the molar activation energy of the circulating water (J/mol). As shown in Fig. 8a, the molecular activation energy of circulating water without magnetic field remained unchanged. The activation energy is the required energy to form a hole. That is to say, be capable of containing a water molecule in the liquid. Thus, the higher the activation energy, the larger the energy required to transform the liquid from a stable to active state [41]. The activation energy curve of circulating water increased at first and then stabilized at 0.27 T. The same behavior was found at higher magnetic field intensity. The results show that activation energy increases with augment of magnetic field intensity. The activation energy of circulating water without magnetic field remained unchanged. This indicates that energy requiring transform to the active state was unchanged. So the circulating water was prone to chemical reaction and calcium and carbonate ions could more easily form calcium carbonate.

Fig. 8b displays the effect of magnetic field on the relative change in the intramolecular energy of circulating water. As shown in the figure, the intramolecular energy of circulating water without magnetic field hardly changed with increasing of magnetic treatment time. When magnetic field intensity was 0.27 and 0.4 T, the relative change in intramolecular energy declined by small and significant amounts, respectively. With increasing magnetic field intensity, the degree of decline in the relative change in intramolecular energy became increasingly apparent. The above results reveal that magnetic field favorably reduces the intramolecular energy in the circulating water to strengthen the interaction forces between molecules. The viscosity of the liquid increased under the external magnetic field, indicating that the forces among water molecules increases to form more associated hydrated ions. More scale-forming ions were combined with water molecules to form hydrated ions, which further decreased the probability of collisions among scale-forming ions. The reduction inhibits scale formation.

## 4. Conclusions

In this study, we treated circulating water by taking advantage of a synergistic effect between magnetic field and $NH_2$–SH–GO/o-MWCNT composite. The $NH_2$-SH-GO/o-MWCNTs were first prepared and characterized with TEM, FT-IR, and XPS. The synergistic effect between the prepared composite material (as the adsorbent) and magnetic field was used to treat circulating water containing $Pb^{2+}$, $Ca^{2+}$, and phenol. The effect of magnetic field intensity on several parameters could be analyzed including equilibrium adsorption quantities, pH, activation energy, relative variation in intramolecular energy, and proportion of free water. TEM images showed that multi-walled CNTs inserted into GO layers to form the composite material. The occurrence of Si–O bonds in the FT-IR spectra indicates that MPTSconnect with oxygen-containing groups on the surface of CNTs or GO. The molecular activation energy of circulating water remained unchanged without magnetic field. Intramolecular energy of circulating water declined slightly at 0.27 T. The proportion of free water was reduced by magnetic treatment, implying that more scale-forming ions were present as hydrated ions. The combined utilization of magnetic field and $NH_2$–SH–GO/o-MWCNT can inhibit scale formation and promote lead ions adsorption but inhibits phenol adsorption. The method has promising prospects and may be useful in various industrial settings.

## Acknowledgments

The authors are grateful for financial support from the National Natural Science Foundation of China (51304101, 51764039), Scientific and Research Project of Institutions of Higher Learning in Gansu Province (2015B-033), and the

Youth Science and Technology Fund Project of Gansu Province (1606RJYA305), and Doctor research cost of Lanzhou university of technology (061702).

## References

[1] M.A. Barakat, New trends in removing heavy metals from industrial wastewater, Arab. J. Chem., 4 (2011) 361–377.
[2] J.O. Nriagu, Quantitative assessment of worldwide contamination of air water and soils by trace metals, Nature, 333 (1988) 134–139.
[3] M. Xin, Y.H. Tang, W.Y. Christina, The latent causal chain of industrial water pollution in China, Environ. Pollut., 196 (2015) 473–477.
[4] L.L. Jiang, S.J. Li, H.T. Yu, Z.Z. Zhou, X.G. Hou, Amino and thiol modified magnetic multi-walled carbon nanotubes for the simultaneous removal of lead, zinc, and phenol from aqueous solutions, Appl. Surf. Sci., 369 (2016) 398–413.
[5] C. Gabrielli, R. Jaouhari, G. Maurin, Magnetic water treatment for scale prevention, Water Res., 35 (2001) 3249–3259.
[6] B. Mahmoud, M. Yosra, A. Nadia, Effects of magnetic treatment on scaling power of hard waters, Sep. Purif. Technol., 171 (2016) 88–92.
[7] C. Gabrielli, R. Jaouhari, G. Maurin, Magnetic water treatment for scale prevention, Water Res., 35 (2001) 3249–3259.
[8] P. Muchez, M. Corbella, Factors controlling the precipitation of copper and cobalt minerals in sediment-hosted ore deposits: Advances and restrictions, J. Geochem. Explor., 118 (2012) 38–46.
[9] T. Kang, H. Kim, H. Kim, J. Moon, S. Hong, J. Yi, Preparation of novel ceramic membranes modified by mesoporous silica with 3-aminopropyltriethoxysilane (APTES) and its application to $Cu^{2+}$ separation in the aqueous phase, J. Membr. Sci., 301 (2007) 118–125.
[10] J.J. Chuechill, M.W. Beutel, P.S. Burgoon, Evaluation of optimal dose and mixing regime for alum treatment of Matthiesen creek inflow to Jameson lake, Washington, Lake. Reserv. Manage., 25 (2009) 102–110.
[11] P.K. Jal, S. Patel, B.K. Mishra, Chemical modification of silica surface by immobilization of functional groups for extractive concentration of metal ions, Talanta, 62 (2004) 1005–1028.
[12] G.X. Zhao, J.X. Li, X.K. Wang, Kinetic and thermodynamic study of 1-naphthol adsorption from aqueous solution to sulfonatedgraphene nanosheets, Chem. Eng. J., 173 (2011) 185–190.
[13] Y. Shen, Q. Fang, B. Chen, Environmental applications of three-dimensional graphene-based macrostructures: adsorption, transformation, and detection, Environ. Sci. Technol., 49 (2015) 67–84.
[14] S. Iijima, Helical microtubules of graphitic carbon, Nature, 354 (1991) 56.
[15] C.B. Wade, C. Thurman, W. Freas, Preparation and characterization of high efficiency modified activated carbon for the capture of mercury from flue gas in coal-fired power plants, Fuel Process. Technol., 97 (2012) 107–117.
[16] W.J. Yang, P. Ding, L. Zhou, J.G. Yu, X.Q. Chen, F.P. Jiao, Preparation of diamine modified mesoporous silica on multi-walled carbon nanotubes for the adsorption of heavy metals in aqueous solution, Appl. Surf. Sci., 282 (2013) 38–45.
[17] J. Teng, X. Zeng, X. Xu, J.G. Yu, Assembly of a novel porous 3D graphene oxide-starch architecture by a facile hydrothermal method and its adsorption properties toward metal ions, Mater. Lett., 214 (2018) 31–33.
[18] J. Ding, H.W. Sha, S.Y. Zhao, Synthesis of graphene oxide/magnetite chitosan composite and adsorption performance for sulfadiazine, Acta Sci. Circumst., 36 (2016) 3691–3700.
[19] X.P. Zhu, H. Liu, J. Tan, H.W. Liu, C. Feng, Mechanism study of cadmium(II) adsorption on thiol-modified montmorillonite, Rock Min. Anal., 4 (2013) 613–620.
[20] J. Maity, S.K. Ray, Chitosan based nano composite adsorbent-synthesis, characterization and application for adsorption of binary mixtures of Pb(II) and Cd(II) from water, Carbohyd. Polym., 182 (2018) 159–171.
[21] B. Hayatia, A. Malekia, F. Najafib, H. Daraeia, F. Gharibia, G. McKayc, Super high removal capacities of heavy metals ($Pb^{2+}$ and $Cu^{2+}$) using CNT dendrimer, J. Hazard. Mater., 336 (2017) 146–157.
[22] J.Y. Yang, X.Y. Jiang, F.P. Jiao, J.G. Yu, X.Q. Chen, Fabrication of diiodocarbene functionalized oxidized multi-walled carbon nanotube and its aqueous adsorption performance toward Pb(II), Environ. Earth. Sci., 76 (2017) 677–687.
[23] N. Chen, J. Teng, F.P. Jiao, X.Y. Jiang, X. Hao, J.G. Yu, Preparation of triethanolamine functionalized carbon nanotube for aqueous removal of Pb(II), Desal. Water Treat., 71 (2017) 191–200.
[24] J.S. Baker, S.J. Judd, Magnetic amelioration of scale formation, Water Res., 30 (2001) 247–260.
[25] B. Mahmoud, M. Yosra, A. Nadia, Effects of magnetic treatment on scaling power of hard waters, Sep. Purif. Technol., 171 (2016) 88–92.
[26] L.L. Jiang, X.Y. Yao, H.T. Yu, X.G. Hou, Z.S. Zou, F.M. Shen, C.T. Li, Effect of permanent magnetic field on water association in circulating water, Desal. Water Treat., 79 (2017) 152–160.
[27] K. Higashitani, A. Kage, S. Katamura. K. Imai, Effects of magnetic field on formation of $CaCO_3$ particles, J. Coll. Int. Sci., 156 (1993) 90–95.
[28] S. Hummers, R. Offeman, Preparation of graphitic oxide, J. Am. Chem. Soc., 80 (1958) 1339–1339.
[29] A.G. Rinzler, R.E. Smalley, Fullerence pipes, Science, 280 (1998) 1253–1256.
[30] R. Rostamian, H. Behnejad, A comparative adsorption study of sulfamethoxazole onto graphene and graphene oxide nanosheets through equilibrium, kinetic and thermodynamic modeling, Process Saf. Environ., 102 (2016) 20–29.
[31] J. Chen, M. Zhao, Y. Li, Preparation of graphene oxide/multiwalled carbon nanotubes 3D flexible architecture for robust biosensing application, Ceram. Int., 41 (2015) 15241–15245.
[32] D.M. Khan, A. Kausar, S.M. Salman, Buckypapers of polyvinyl chloride/poly (styrene-co-maleic anhydride) blend intercalated graphene oxide-carbon nanotube nanobifiller: Physical property exploration, Fuller. Nanotub. Car. N., 24 (2016) 202–212.
[33] P.A.M. Mourao, P.J.M. Carrott, M.M.L. Carrott, Application of different equations to adsorption isotherms of phenolic compounds on activated carbons prepared from cork, Carbon, 44 (2006) 2422–2429.
[34] C.V. Pham, M. Eck, M. Krueger, Thiol functionalized reduced graphene oxide as a base material for novel graphene-nanoparticle hybrid composites, Chem. Eng. J., 231 (2013) 146–154.
[35] E.V. Jelenkovic, S. To, M.G. Blackford, XPS and TEM study of deposited and Ru-Si solid state reaction grown ruthenium silicides on silicon, Mat. Sci. Semicon. Proc., 40 (2015) 817–821.
[36] S. Yagi, M. Nambu, C. Tsukada, Spectral studies on sulfur poisoning of Pd/Mg 6Ni by NEXAFS and XPS, Appl. Surf. Sci., 267 (2013) 45–47.
[37] M. Chandran, M. Shasha, S. Michaelson, Incorporation of low energy activated nitrogen onto HOPG surface: Chemical states and thermal stability studies by in-situ XPS and Raman spectroscopy, Appl. Surf. Sci., 382 (2016) 92–201.
[38] H. Hosoda, H. Mori, N. Sogoshi, N. Sogoshi, A. Nagasawa, S. Nakabayashi, Refractive indices of water and aqueous electrolyte solutions under high magnetic fields, J. Phys. Chem. A, 108 (2004) 1461–1464.
[39] L.L. Jiang, J.L. Zhang, D.K. Li, Effects of permanent magnetic field on calcium carbonate scaling of circulating water, Desal. Water Treat., 53 (2015) 1275–1285.
[40] W.W. Li, M.R. Li, Adsorption mechanism of $Pb^{2+}$, $Cd^{2+}$ and$Cu^{2+}$ onto bamboo-based magnetic-carbon, Acta Scien. Circum., 34 (2014) 938.
[41] L.L. Jiang, X.Y. Yao, H.T. Yu, X.G. Hou, Z.S. Zou, F.M. Shen, C.T. Li, Effect of permanent magnetic field on scale inhibition property of circulating water, Water Sci. Technol., 76 (2017) 1981-1991.